

## Article

# Interface Strengthening and Toughening Mechanism of Hot Rolled Multilayer TWIP/40Si2CrMo Steels

Mingchao Dong <sup>1</sup>, Zhuoyu Li <sup>1</sup>, Baoxi Liu <sup>1,2,\*</sup>, Cuixin Chen <sup>1,2</sup>, Wenxing Yu <sup>3,\*</sup>, Bo Yang <sup>1</sup> and Fuxing Yin <sup>1,2,4</sup> <sup>1</sup> School of Materials Science and Engineering, Hebei University of Technology, Tianjin 300130, China<sup>2</sup> Research Institute for Energy Equipment Materials, Tianjin Key Laboratory of Materials Laminating Fabrication and Interfacial Controlling Technology, Tianjin 300000, China<sup>3</sup> School of Mechanical Engineering, Hebei University of Technology, Tianjin 300130, China<sup>4</sup> Institute of New Materials, Guangdong Academy of Sciences, Guangzhou 510651, China

\* Correspondence: liubaoxiliubo@126.com (B.L.); yuwenxing128323@163.com (W.Y.);

Tel.: +86-156-2003-1851 (B.L.)

**Abstract:** Layered metal composites play an increasingly important role in aerospace, automotive, and nuclear energy. Compared with a single metal or alloy, the layered metal composite exhibits an excellent strong-plastic matching effect. In this paper, multilayer TWIP/40Si2CrMo steels with different hot rolling reductions were successfully fabricated by the vacuum hot rolling. The results show that the multilayer steels can improve the lower yield strength of TWIP steel and lower the fracture elongation of 40Si2CrMo steel. In addition, with the increase of the hot rolling reduction, the mechanical properties and interfacial bonding strength of multilayer steels were improved, while the size and number of interfacial oxides decrease, and the fracture mode was also changed. This shows that a higher hot rolling reduction will promote the breakage of the interface oxides and make them appear dispersed, thereby improving the bonding strength of the interface, effectively suppressing the delamination and local necking of the multilayer steel, and making the multilayer steel show a higher ability of uniform plastic deformation. At the same time, under the dual action of layer thickness scale and interface strengthening effect, the brittle layer of multilayer steel presents a multiple tunnel crack mode. It was beneficial to alleviate the stress concentration and further improve the strengthening and toughening effect of multilayer steel.

**Keywords:** vacuum hot rolling; multilayer steel; reduction; interface; strengthening and toughening



**Citation:** Dong, M.; Li, Z.; Liu, B.; Chen, C.; Yu, W.; Yang, B.; Yin, F. Interface Strengthening and Toughening Mechanism of Hot Rolled Multilayer TWIP/40Si2CrMo Steels. *Crystals* **2022**, *12*, 1367. <https://doi.org/10.3390/cryst12101367>

Academic Editor: Pavel Lukáč

Received: 5 September 2022

Accepted: 21 September 2022

Published: 27 September 2022

**Publisher's Note:** MDPI stays neutral with regard to jurisdictional claims in published maps and institutional affiliations.



**Copyright:** © 2022 by the authors. Licensee MDPI, Basel, Switzerland. This article is an open access article distributed under the terms and conditions of the Creative Commons Attribution (CC BY) license (<https://creativecommons.org/licenses/by/4.0/>).

## 1. Introduction

It was well known that TWIP steel has high plasticity and induces deformation twins in (FCC) $\gamma$  austenite matrix under an external load, which significantly delays the necking of steel. In addition, TWIP steel also has excellent formability, high strain hardening, and high energy absorption capacity [1]. Therefore, TWIP steel was considered the second generation of advanced high-strength steel (AHSS), which has been widely used in lightweight materials for automobiles. However, the low yield strength limits its further application. To solve these problems, severe plastic deformation (SPD) methods [2–4], such as cold rolling, accumulative roll bonding, caliber rolling, and equal channel angular pressing were used to achieve strengthening. Although these methods can effectively improve the yield strength of TWIP steel, they will lead to a rapid decrease in plasticity. In addition, the strain stability of severely deformed microstructure is still an unsolved problem. Compared with TWIP steel, 40Si2CrMo medium carbon low alloy steel especially after quenching has a higher yield strength and tensile strength, but a large loss of plasticity limits its practical industrial application. At present, there are few studies on improving the plasticity of 40Si2CrMo medium carbon low alloy steel, and there is no systematic research work.

The multilayer structure is composed of an alternating high strength (hard) layer and high plastic (soft) layer, which can increase the mechanical properties of the material and

has been widely used in industrial production [5]. On one hand, the stress and strain of the soft phase layer and the hard phase layer were redistributed during deformation, and the higher load of the soft phase layer can be transferred to the hard phase layer through the interface. On the other hand, its plasticity can also be enhanced by the interface energy dissipation mechanism to improve damage tolerance [6]. Pozuelo et al. [7] successfully manufactured 70 layers of multilayer steels of ultra-high carbon steel and low carbon steel that were alternately stacked by hot rolling. They found that the impact absorption energy of multilayer steel is 70 times and 1.5 times that of the two constituent materials, respectively. Kang et al. [8] studied the layered clad steel plate that was composed of IF steel-TWIP steel-IF steel and found that each layer would produce uniform strain during hot rolling, which ensured the consistency of layer thickness. Grain boundary hardening and deformation twinning of TWIP steel improved the mechanical properties of the material. Toshihiko et al. [9] found that multilayer steel has good comprehensive mechanical properties through interface delamination and tunnel crack toughening mechanisms in the process from development to application. Many studies had shown that the physical, chemical, and mechanical properties of multilayer steels were much better than those of constituent metal materials [10,11]. As shown in Figure 1, most of the component materials were located below the “banana curve” (strength-toughness trade off relationship curves), while the multilayer steels were significantly higher than the banana curve and have strength-toughness synergism. Therefore, the metal multilayer composites that are composed of alternating metals have been recognized as the crucial role to solving the strength-toughness trade-off relationship in previous studies.

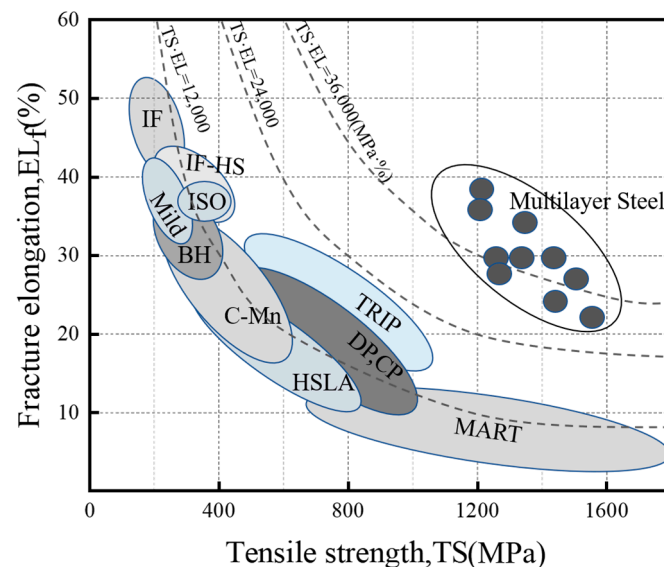


**Figure 1.** Strength-plastic relationships of monolithic metal materials and multilayer steels.

It had been reported that the mechanical properties of multilayer steels generally follow the mean rule, but the elongation deviates from the mean rule due to interfacial delamination. Song et al. [12] found that the fracture toughness of biomimetic laminated ceramics was lower than that of natural shells. One of the main reasons was that the interfacial delamination crack length that was produced by biomimetic laminated ceramics was about four times longer than the natural laminated shells. However, if the multilayer steel has a strong bonding interface when the hard phase layer has a tendency of local necking, the soft phase layer will produce a strong necking-inhibition effect on the hard phase layer through the interface, until the fracture will not produce obvious tunnel cracks and interface delamination cracks, which has a strong coordination ability of interface deformation [13,14]. Therefore, it was expected to form a suitable interface, which not only

maintains a certain bond strength but also has slight delamination to prevent necking or cracking in the hard phase layer, thereby obtaining higher strength and ductility.

In this paper, multilayer TWIP/40Si2CrMo steels were fabricated by vacuum hot rolling with three different hot rolling reductions. The multilayer steels not only inherited the high plasticity and high work hardening ability of TWIP steel but also continued the high yield strength of 40Si2CrMo steel. The microstructure and mechanical properties of multilayer TWIP/40Si2CrMo steels with three hot rolling reductions were studied, the evolution of interfacial bonding strength and its effect on the strength and ductility of the multilayer steels were analyzed, and the strengthening and toughening mechanism of the interfacial area were clarified, which provided the experimental and theoretical basis for high-quality multilayer steels.

## 2. Materials and Methods

The multilayer steel consists of 120 layers of alternating Fe-18Mn-1.5Al-0.6C TWIP steel and 40Si2CrMo medium carbon low alloy steel. The chemical compositions of the two steels are listed in Table 1. The fabricated process of multilayer TWIP/40Si2CrMo steel mainly includes three stages: packing billet, vacuum sealing, and hot rolling. The specific fabrication process diagram is shown in Figure 2. Firstly, steel sheets with a thickness of 0.5 mm were cut on TWIP and 40Si2CrMo ingots. The sample surface was polished with SiC sandpaper and then cleaned with acetone and alcohol to remove stains and rust. The clean TWIP and 40Si2CrMo steel sheets were alternately stacked in the manner of “TWIP/40Si2CrMo/TWIP/40Si2CrMo...” into the carbon steel box, as shown in Figure 2a. A layer of isolation cloth was covered on the outermost side, which was to prevent carbon diffusion and to easily separate the multilayer composite matrix from the carbon steel box after hot rolling. Secondly, a hollow circular tube with a 10 mm diameter hole was welded to the side of the carbon steel box wall, and the rest was welded to seal. The billet was vacuum treated by a vacuum pump, when the vacuum degree of the billet was less than  $10^{-2}$  pa, the hollow circular tube was clamped with a hydraulic clamp to isolate the outside air and achieve a predetermined vacuum degree inside the billet. The billet to be rolled as shown in Figure 2b. Finally, the billets were heated in a box-type heating furnace at 1200 °C for 1 h for homogenization treatment and then rolled at different hot rolling reductions, respectively. The total thickness of multilayer steels with hot rolling reductions of 80%, 90%, and 95% were 12, 6, and 3 mm, respectively.

**Table 1.** The chemical compositions of TWIP steel and 40Si2CrMo steel [wt.%].

Element	C	Mn	Al	Si	Cr	Mo	Fe
Fe-18Mn-1.5Al-0.6C	0.6	18.0	1.5	-	-	-	79.9
40Si2CrMo	0.4	-	-	2.0	1.0	1.0	95.6

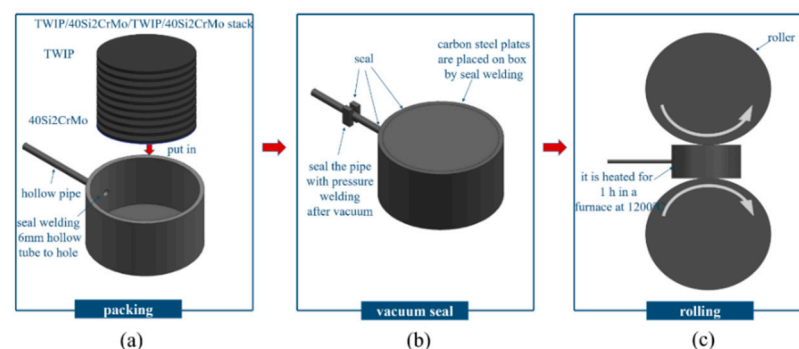


**Figure 2.** The fabricated process of hot rolled multilayer TWIP/40Si2CrMo steel: (a) packing billet; (b) vacuum sealing; (c) hot rolling.

The microstructure and interface characteristics of multilayer steels were analyzed by an AxioVertA1 optical microscope (OM), JSM-7100F scanning electron microscope (SEM) that was equipped with electron back scatter diffraction (EBSD), and transmission electron microscope (TEM). The distribution characteristics, morphologies, and sizes of interfacial compounds in multilayer steels were analyzed by The JXA-8530F electron probe microanalyzer (EPMA). The DUH211S microhardness measurement system was carried out to measure the Vickers' hardness with HV0.1 and hold pressure for 10 s. The XRD was carried out at room temperature in a Rigaku (DMAX2500) diffractometer with a Cu target and a step size of  $0.02^\circ$ . Tensile and shear properties were tested with an AGS-50kNX tensile testing machine with a strain rate of  $1.67 \times 10^{-3} \text{ s}^{-1}$ , and the tensile and shear fracture morphologies of the multilayer steels were observed and analyzed by scanning electron microscope. The dimensions of the tensile specimens and shear specimens are shown in the Figure 3.

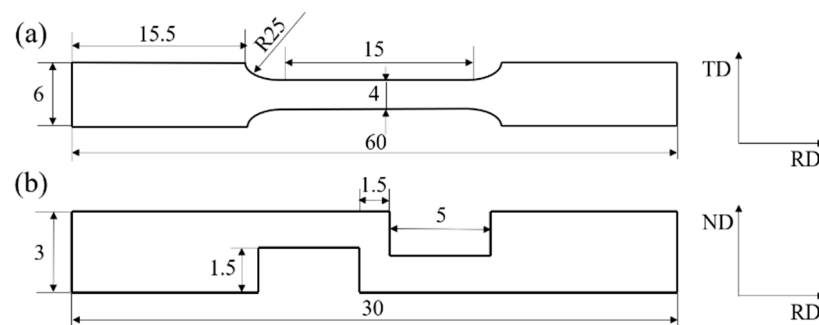
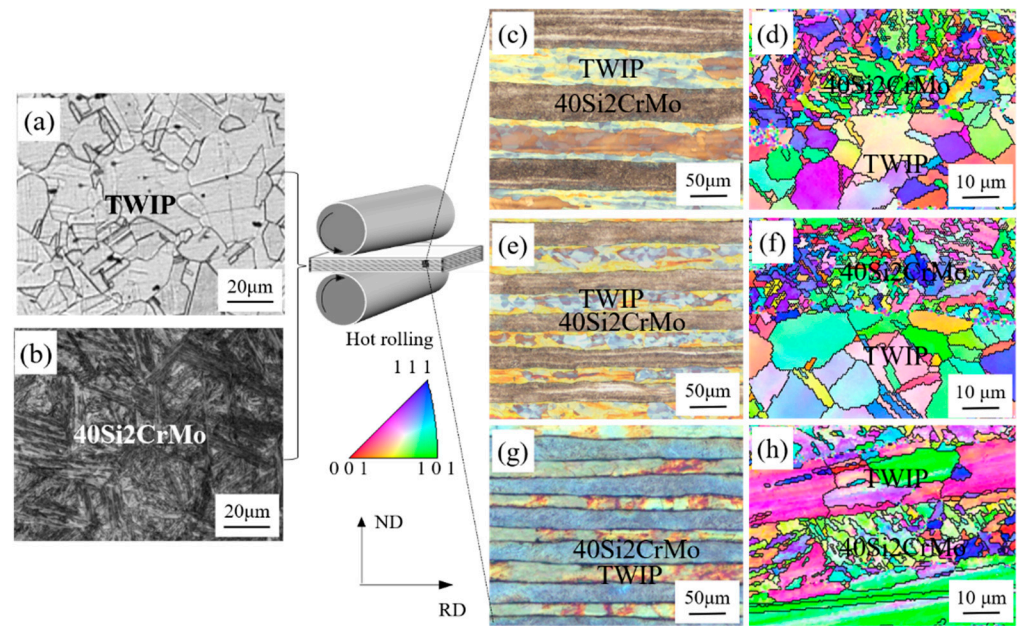


Figure 3. Schematic diagram of (a) tensile specimen; (b) tensile-shear specimen.

### 3. Results

Figure 4 shows the microstructures of the original monolithic steels and the hot rolled multilayer steels. The microstructure of the original TWIP steel was equiaxed austenite, as shown in Figure 4a. Due to the addition of alloy elements such as Si, Cr, and Mo to improve hardenability, a large number of needle-like structures, which were typical of lower bainite were distributed in the original 40Si2CrMo steel, as shown in Figure 4b. All TWIP/40Si2CrMo multilayer steels have straight interfaces with no voids and microcracks, and a relatively uniform layer thickness, indicating that the multilayer steels have well-bonded interfaces and high deformation coordination, as shown in Figure 4c–h. In addition, with the increase of hot rolling reduction, the thickness of multilayer steel decreases, and the grains lengthen along the rolling direction. The grain sizes of three kinds of multilayer steels are shown in Table 2. It can be found that the grain size decreases slightly with the increase of hot rolling reduction, but the grain size of the TWIP steel layer was larger than that of the 40Si2CrMo steel layer. The study found that the decrease of hot rolling reduction can contribute to the plasticity of multilayer steel through the layer thickness scale effect [15,16] and that the graded grain structure will generate strong back stress and work hardening [17,18]. For example, Hao Ding et al. fabricated multilayer titanium with a gradient/lamellar structure and harmonic mixed crystal structure by hot pressing sintering and rolling composite process. The synergistic deformation behavior and strain gradient effect of the multi-stage structure were analyzed by OM-DIC, SEM-DIC, EBSD-DIC, and TEM in situ/semi-in situ, the back stress strengthening mechanism in the kinematic hardening mode is revealed by cyclic loading [19].

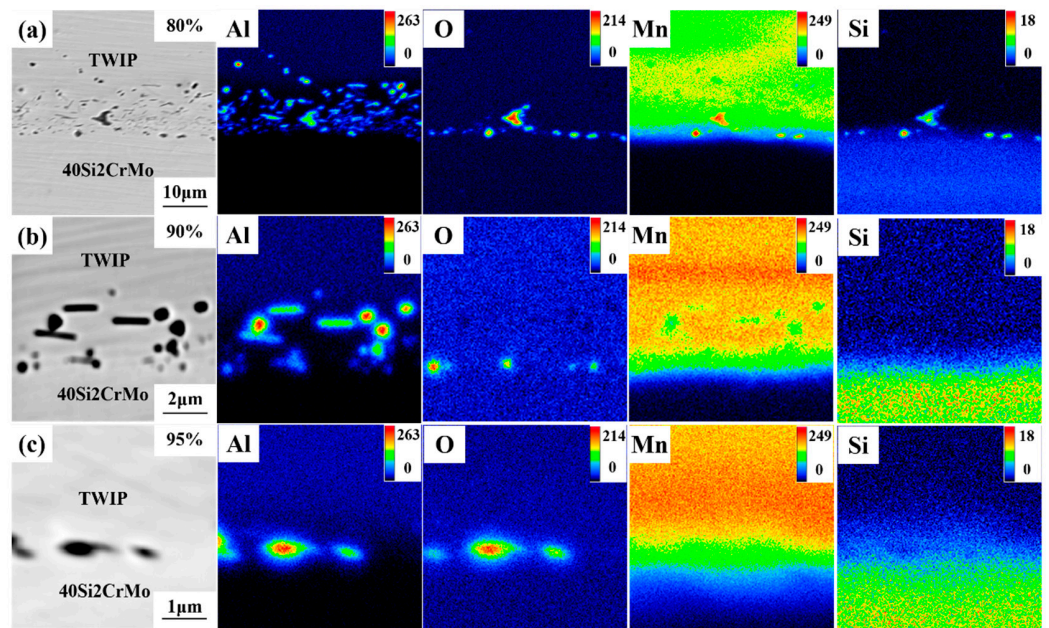


**Figure 4.** The microstructures of TWIP, 40Si2CrMo, and the multilayer steels with three hot rolling reductions: (a) TWIP steel; (b) 40Si2CrMo steel; (c,d) the reduction is 80%; (e,f) the reduction is 90%; (g,h) the reduction is 95%. RD: Parallel to the rolling direction; ND: Perpendicular to the rolling direction.

**Table 2.** Grain sizes of the constituent layer of multilayer TWIP/40Si2CrMo steel with three hot reductions.

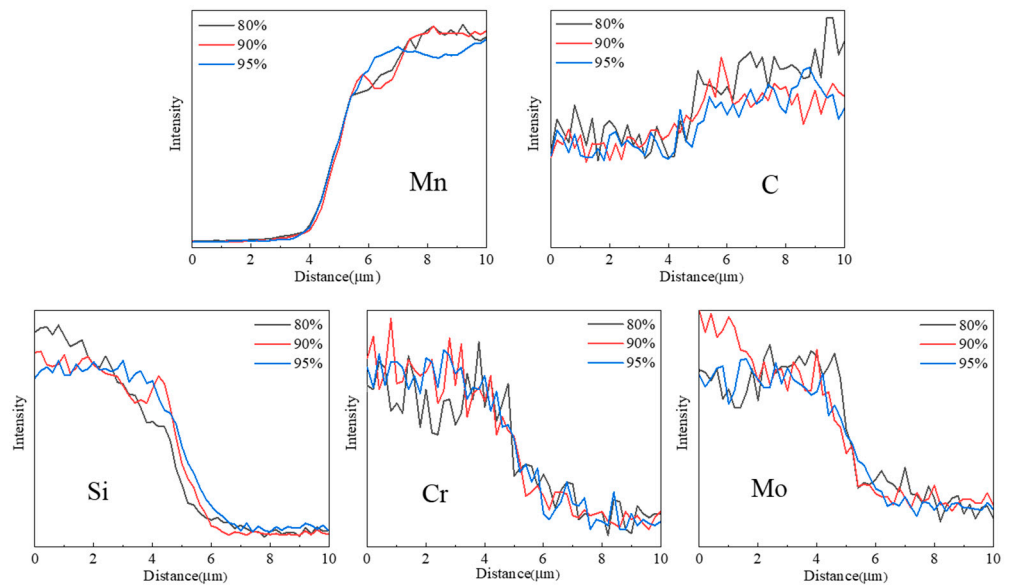
Hot Rolling Reduction	TWIP Steel ( $\mu\text{m}$ )	40Si2CrMo Steel ( $\mu\text{m}$ )
80%	17.2	8.3
90%	15.9	7.7
95%	15.0	7.2

Figure 5 shows the element distributions of multilayer TWIP/40Si2CrMo steels with different hot rolling reductions. It can be seen that the interface of all multilayer steels mainly forms the oxide of Al, indicating that the Al oxidation cannot be completely avoided in multilayer TWIP/40Si2CrMo steel under the condition of  $10^{-2}$  Pa vacuum degrees. When the multilayer steel was in the heating process, the active Al in TWIP steel was easy to react with oxygen in the air to form  $\text{Al}_2\text{O}_3$  [20]. When the hot rolling reduction was 80%, the interfacial oxides of the multilayer steel were larger in size and quantity. With the increase of the hot rolling reduction, the layer thickness decreases, and the size and quantity of the interfacial oxide gradually become smaller, which was caused by the crushing of Al oxides under the action of rolling force, friction, and shearing force. The larger size of interfacial oxide will lead to the phenomenon of crack nucleation and expansion along the oxide boundary in the deformation process of multilayer steel, thereby causing serious delamination failure of the multilayer steel, so the reduction of the size of the hard oxides at the interface was beneficial to the bonding of the heterointerface, along with lowering the stress concentration which prevents crack initiation and propagation.



**Figure 5.** EPMA surface scanning of the element distributions of multilayer TWIP/40Si2CrMo steels with different hot rolling reductions: (a) 80%; (b) 90%; (c) 95%.

There were different degrees of element diffusion in the multilayer steels with three hot rolling reductions. The specific diffusion distances of the elements are shown in Figure 6 and Table 3. It can be seen that the diffusion distance of elements such as C, Mn, Si, Cr, and Mo decreases with the increase of hot rolling reduction, which leads to the thinning of the diffusion layer thickness of the multilayer steel. In the process of hot rolling, the diffusion of elements along the interface will reduce the mechanical properties of the multilayer steel. To obtain excellent mechanical properties, a narrower transition layer was often required. So, when the reduction was 95%, the thickness of the diffusion layer of the multilayer steel was reduced to about 2  $\mu\text{m}$ , and the highest strength-plasticity match was obtained.



**Figure 6.** EPMA line scan of the element distributions of multilayer TWIP/40Si2CrMo steels with different hot rolling reductions.

**Table 3.** The element diffusion distances of multilayer TWIP/40Si2CrMo steels with different hot rolling reductions.

Element	80% ( $\mu\text{m}$ )	90% ( $\mu\text{m}$ )	95% ( $\mu\text{m}$ )
Mn	5.0	4.4	3.8
C	2.6	2.8	1.4
Si	4.4	3.0	2.8
Cr	4.4	4.4	4.2
Mo	3.6	3.2	3.2

Figure 7 shows the microhardness values of multilayer TWIP/40Si2CrMo steels with different hot rolling reductions. It was obvious that the hardness of the TWIP steel layer was lower than that of the 40Si2CrMo steel layer. For example, when the hot rolling reduction was 80%, the hardness of the TWIP steel layer was about 1.5 times that of the 40Si2CrMo steel layer. This difference in hardness will also show a difference in deformation coordination, which results in a change in fracture mode. In addition, with the increase of hot rolling reduction, the hardness of the TWIP steel layer and 40Si2CrMo steel layer both increased. This was because the number of dislocations in the constituent layers increases, and the packing and winding of dislocations further hinder the movement of dislocations, resulting in work hardening, which increases the hardness of the constituent layer [21,22].

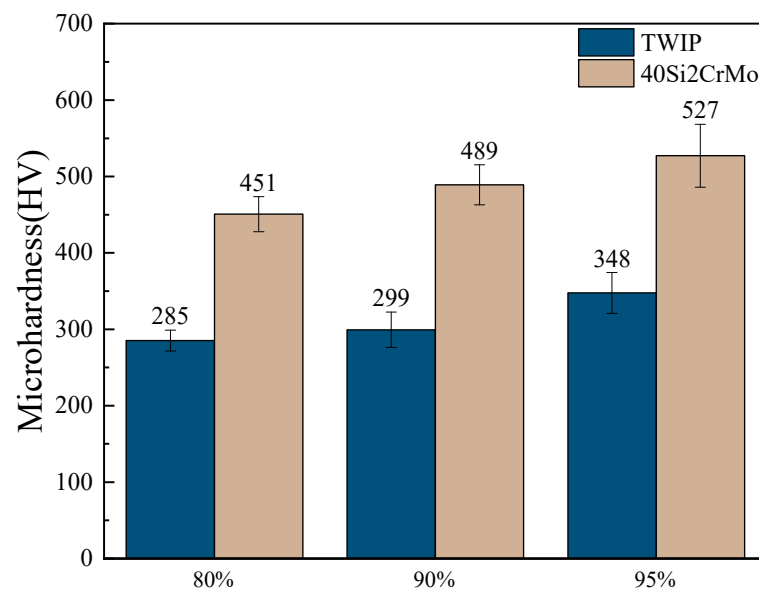
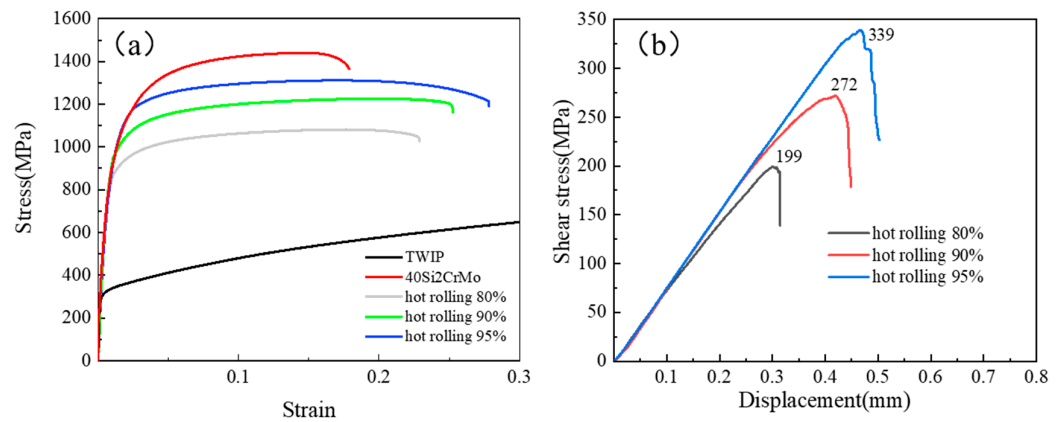
**Figure 7.** Microhardness values of multilayer TWIP/40Si2CrMo steels with different hot rolling reductions.

Figure 8a shows the engineering stress-strain curves of hot rolling multilayer TWIP/40Si2CrMo steels. The specific values are shown in Table 4. It can be seen that the yield strength of TWIP steel was lower, only 321 MPa, but has a higher work-hardening ability, while 40Si2CrMo steel has higher yield strength, but its fracture elongation was only 17.8%. The multilayer steels that were made by hot rolling successfully inherit the advantages of the two-component layers. The tensile strength of the multilayer steel with the hot rolling reduction of 80% was 1081 MPa and the fracture elongation was 22.9%. When the rolling reduction was increased to 95%, the tensile strength, yield strength, and fracture elongation of the multilayer steel were increased to 1311 MPa and 1148 MPa, and 27.8% respectively. Interestingly, with the increase of reduction, the strength and the fracture elongation simultaneously increase, which breaks the “strength-toughness” trade off relationship of traditional materials. The improvement of the tensile strength of multilayer steel was mainly due to the joint action of grain refinement and work hardening of the TWIP steel

layer, and the main reason for the increase of fracture elongation may be the interfacial toughening and layer thickness scale effect.



**Figure 8.** (a) Engineering stress-strain curve and (b) tensile-shear stress-displacement curves of multilayer TWIP/40Si2CrMo steels with different hot rolling reductions.

**Table 4.** Mechanical properties of multilayer TWIP/40Si2CrMo steels with different hot rolling reductions.

Rolling Reduction	$\sigma_s$ (MPa)	$\sigma$ (MPa)	$\epsilon$ (%)	Shear Strength (MPa)
TWIP	321	769	60.8	-
40Si2CrMo	1136	1440	17.8	-
hot rolling 80%	865	1081	22.9	199
hot rolling 90%	1028	1226	25.3	272
hot rolling 95%	1148	1311	27.8	339

Note:  $\sigma_s$  is the yield strength,  $\sigma$  is the tensile strength, and  $\epsilon$  is the fracture elongation.

The interfacial bonding strength plays a very important role in the strength and plasticity of multilayer steels, and it can be evaluated by measuring the relative sliding resistance of the interface. When the tensile-shear stress reaches the maximum bonding strength of the interface, the heterogeneous metal slips relatively, which leads to the separation of the interface. Figure 8b shows the tension shear stress-displacement curves of multilayer TWIP/40Si2CrMo steels with three hot rolling reductions. When the hot rolling reductions were 80%, 90%, and 95%, the shear strength of multilayer steels were 199 MPa, 272 MPa, and 339 MPa, respectively, indicating that the increase of the hot rolling reduction will improve the interface bonding strength of the multilayer steel. This was due to the combined effect of the reduction of the interfacial diffusion layer and the crushing of interfacial oxides of the multilayer steel under a larger rolling reduction. Figure 9 shows the shear fracture morphologies of multilayer steel with different hot rolling reductions. As shown in Figure 9a, the specimen with the hot rolling reduction of 80% fractures along the interface and has many interfacial delamination cracks. The shear specimen with a reduction of 90% also fractured along the interface straightly, while the crack deflection phenomenon occurred in the multilayer steel with the reduction of 95%, which impedes part of the stress and improves the interfacial bonding strength of the multilayer steel.

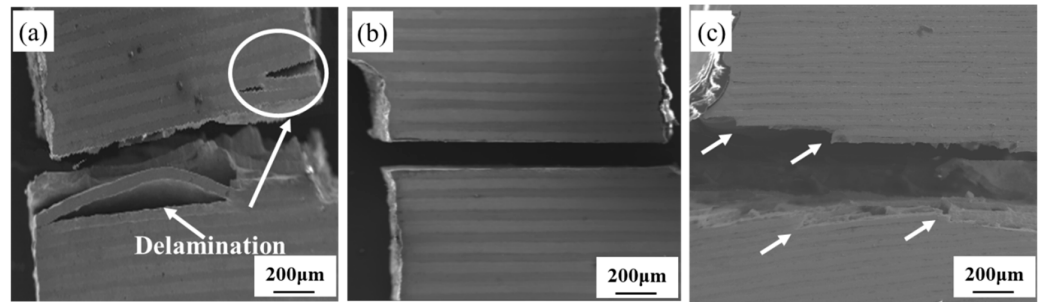


**Figure 9.** Tensile-shear fracture morphologies of the multilayer TWIP/40Si2CrMo steels with different hot rolling reductions: (a) 80%; (b) 90%; (c) 95%.

Figure 10 shows the tensile fracture morphology of multilayer TWIP/40Si2CrMo steels with different hot rolling reductions. Figure 10a,d shows the multilayer steel with the hot rolling reduction of 80% has an obvious delamination fracture, and there were a large number of holes (some oxides were distributed near the holes; it was determined to be the  $\text{Al}_2\text{O}_3$  by EDS analysis, as shown in Figure 11). The larger oxide that formed at the interface will produce voids and stress concentration in the deformation process, which makes the crack nucleate and propagate in the pore area of the oxide, resulting in obvious interface delamination. Delamination made the interface unstable before the necking of the whole steel plate, which leads to the sudden fracture of multilayer steel [23]. The multilayer steel with the hot rolling reduction of 90% has lighter interfacial delamination. This was because the crack was deflected and formed “Z” type multiple propagation paths releasing the stress concentration at the interface and reducing the crack propagation driving force as shown in Figure 10e. The delamination cracks at the interface of the multilayer steel with a hot rolling reduction of 95% were shorter as shown in Figure 10c,f. With the increase of the hot rolling reduction, the delamination phenomenon gradually weakened and the interfacial bonding strength gradually increased. In addition, there were many “tunnel cracks” in the 40Si2CrMo steel layer, which leads to crack passivation. It has been reported that a plastic zone will be formed near the tunnel crack [24], which will help to dissipate energy, reduce the stress concentration at the crack tip, effectively restrain the necking of the hard layer, and improve the plasticity of the multilayer steel.

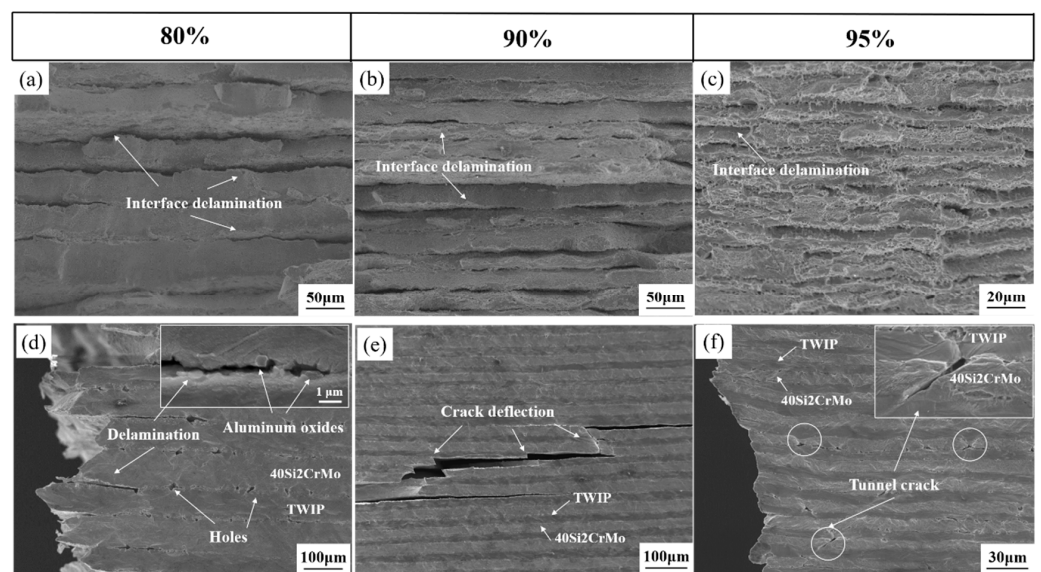


**Figure 10.** Tensile fracture morphologies of multilayer TWIP/40Si2CrMo steels with different hot rolling reductions: (a–c) the front fracture; (d–f) the side fracture.

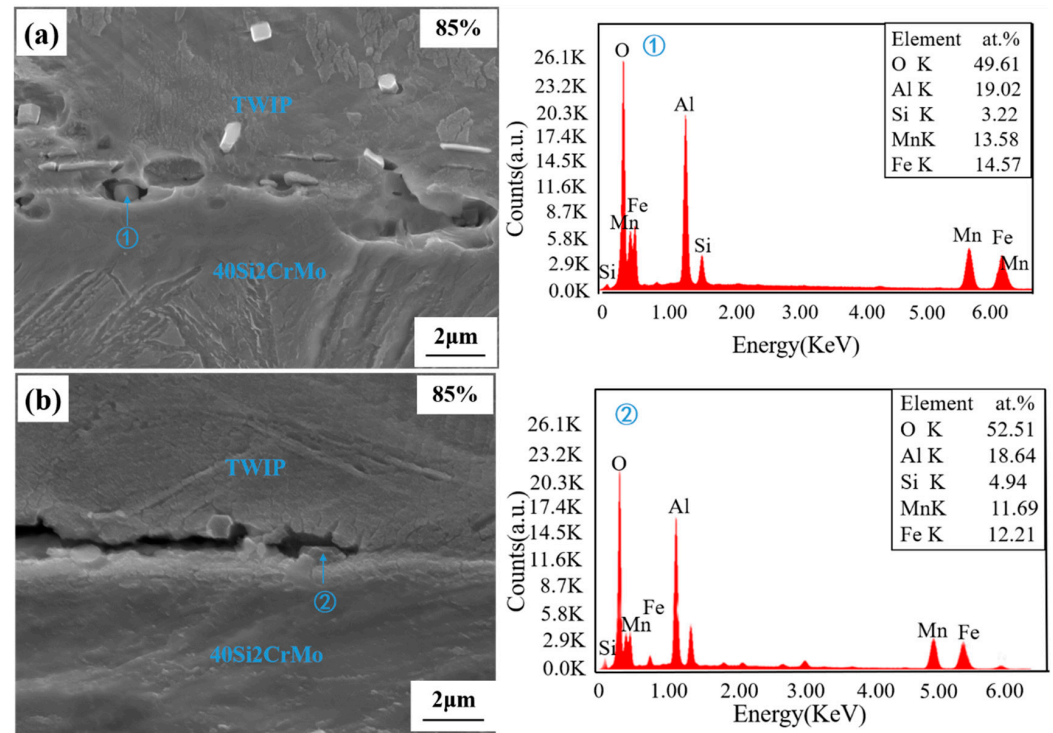


**Figure 11.** EDS spectra of multilayer steel with a hot rolling reduction of 80%: (a) before the tensile test; (b) after the tensile test.

#### 4. Discussion

Figure 12 shows the X-ray diffraction patterns of multilayer steels with different hot rolling reductions. In previous studies, we found that in the process of increasing reduction, the dislocations of the multilayer steels were increased and entangled, which enhances the elastic interaction between the dislocations and makes the dislocation slip difficult, thus improving the strength and plasticity of the multilayer. The specific dislocation density is related to the average crystallite size ( $D$ ) and micro-strain ( $\epsilon_{s0}^2$ ). Crystallite size and micro-strain can be estimated according to Equations (1) and (2) [25]:

$$D = \frac{K\gamma}{\beta_s \cos \theta} \quad (1)$$

$$\frac{\beta_s \cos \theta}{\lambda} = \frac{2 \langle \epsilon_{s0}^2 \rangle \sin \theta}{\lambda} + \frac{K}{d'} \quad (2)$$

where  $K$  is a dimensionless constant,  $K = 1$ ;  $\gamma$  is the wavelength of X-ray,  $\gamma \approx 0.154056$  nm;  $\theta$  is the Bragg angle;  $\lambda$  is the wavelength of the ray  $K\alpha_1$ ,  $\lambda \approx 0.15418$  nm; and  $d'$  is the average grain size.  $\beta_s$  stands for the full width at the half maximum height (FWHM) of the  $K\alpha_1$  line with the correction of instrumental line broadening. The FWHM values are measured  $\gamma$ -Fe(111) and  $\alpha$ -Fe(110) reflections, and they can be calculated by the following equation:

$$\beta_s = \beta_m^2 - \beta_\gamma^2 \quad (3)$$

where  $\beta_m$  is the FWHM value of the  $K\alpha_1$  line of rolled multilayer TWIP/40Si2CrMo steels and  $\beta_\gamma$  is the FWHM value of the instrument. Here is the measured value of the sample after full recrystallization at 1200 °C.

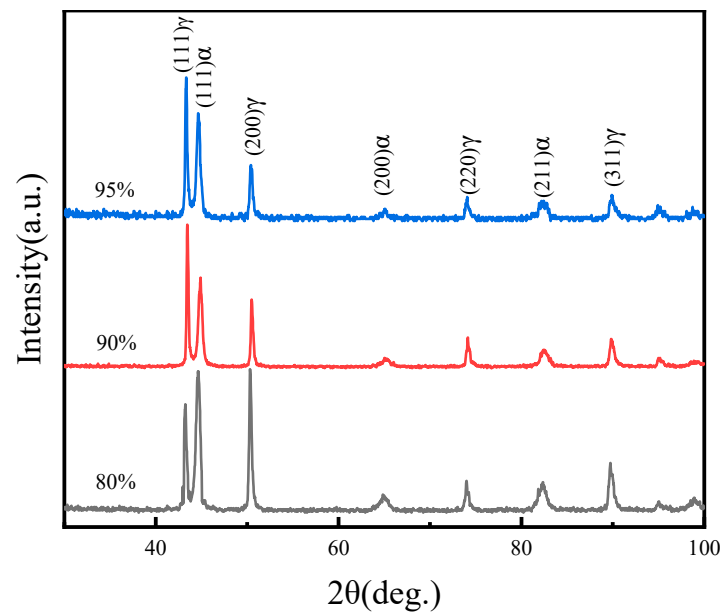


**Figure 12.** XRD patterns of TWIP/40Si2CrMo multilayer steels at different hot rolling reductions.

The dislocation density is calculated as shown in the equation:

$$\rho = \frac{3(2\pi)^{\frac{1}{2}} \langle \epsilon_{s0}^2 \rangle}{Db} \quad (4)$$

where  $b$  is the Burgers vector,  $b = 2.5 \times 10^{-7}$  mm.

The dislocation densities in TWIP and 40Si2CrMo layers of multilayer steels with different hot rolling reductions were shown in Table 5. With the increase of hot rolling reduction, the dislocation density increases slightly and the dislocation density of the 40Si2CrMo steel layer is higher than that of the TWIP steel layer. The contribution of dislocation to material strengthening in the TWIP steel layer and the 40Si2CrMo steel layer was according to the equation:

$$\sigma_{\text{dis}} = \alpha M G b \rho^{\frac{1}{2}} \quad (5)$$

where  $\sigma_{\text{dis}}$  is the contribution value of dislocation density;  $\alpha$  is a constant,  $\alpha = 2$ ;  $M$  is a constant,  $M = 2.9$  [26];  $G$  is the shear modulus; and  $G = 7.1 \times 10^4$  MPa. The calculation results are summarized in Table 5. It can be found from the calculation that with the increase of hot rolling reduction, the contribution of dislocation density of multilayer steel to material strengthening increases slightly. That is to say, in addition to dislocation strengthening, there are other strengthening methods that lead to the improvement of material strength.

**Table 5.** The full width at half maximum (FWHM), dislocation densities, and contribution of dislocation to strength for multilayer TWIP/40Si2CrMo steels with different warm rolling reductions.

Reduction	Composition	Dislocation Density ( $\text{mm}^{-2}$ )	Contribution of Dislocations to Strength (Mpa)
80%	TWIP	$5.7 \times 10^6$	245.8
	40Si2CrMo	$2.0 \times 10^7$	460.4
90%	TWIP	$6.2 \times 10^6$	256.3
	40Si2CrMo	$2.1 \times 10^7$	471.8
95%	TWIP	$7.2 \times 10^6$	276.2
	40Si2CrMo	$2.2 \times 10^7$	478.5

In order to deeply analyze the contribution of each reinforcement, related theoretical calculations were introduced. The yield strength can be calculated according to the following equation [27]:

$$\sigma_{0.2} = \sigma_0 + \Delta\sigma_{\text{refin}} + \Delta\sigma_{\text{twin}} \quad (6)$$

where  $\sigma_0$  is the contribution of the original material to the yield strength;  $\Delta\sigma_{\text{refin}}$  is the value of grain refining; and  $\Delta\sigma_{\text{twin}}$  is the value of strain-induced twinning.

$$\sigma_0 = f_{\text{TWIP}}\sigma_{\text{TWIP}} + f_{40\text{Si2CrMo}}\sigma_{40\text{Si2CrMo}} \quad (7)$$

where  $f_{\text{TWIP}}$  and  $f_{40\text{Si2CrMo}}$  are the volume fractions of TWIP steel and 40Si2CrMo steel, respectively;  $f_{\text{TWIP}} = f_{40\text{Si2CrMo}} = 0.5$ ;  $\sigma_{\text{TWIP}}$  and  $\sigma_{40\text{Si2CrMo}}$  are the yield strength of the original materials.

$$\Delta\sigma_{\text{refin}} = \frac{f_{\text{TWIP}}K_{\text{TWIP}}}{d_{\text{TWIP}}^{1/2}} + \frac{f_{40\text{Si2CrMo}}K_{40\text{Si2CrMo}}}{d_{40\text{Si2CrMo}}^{1/2}} \quad (8)$$

where  $K_{\text{TWIP}}$  and  $K_{40\text{Si2CrMo}}$  are the Halls–Petch constants of TWIP steel and 40Si2CrMo steel, respectively.  $K_{\text{TWIP}} = 0.445 \text{ GPa}\cdot\text{m}^{1/2}$  [28], The Hall–Petch parameters of 40Si2CrMo steel takes the value of ordinary low alloy steel,  $K_{40\text{Si2CrMo}} = 0.24 \text{ GPa}\cdot\text{m}^{1/2}$  [29]. The  $d_{\text{TWIP}}$  and  $d_{40\text{Si2CrMo}}$  are the average grain diameters of the TWIP layer and 40Si2CrMo layer, respectively.

$$\Delta\sigma_{\text{twin}} = \frac{f_{\text{TWIP}}K_{\text{TWIP}}}{d_{\text{TWIP}}^{1/2}} \quad (9)$$

The corresponding values for each item are shown in Table 6. The calculated values of the rolling reduction of 80% is approximated to the experimental results. However, the calculated value of 90% and 95% reductions of multilayer steel were smaller than the measured value. This may be because the contribution of dislocation density and the effect of interfacial bonding strength on the material are not considered. As shown in Table 5, with the increase of reduction, dislocation density also plays an indispensable role in the improvement of material yield strength. That is to say, with the increase of hot rolling reduction, the increase in the strength of multilayer steel was the joint effect of grain refinement strengthening, twin hardening, interface enhancement, and dislocation strengthening.

**Table 6.** The contributions of grain refining and strain-induced twinning, and the calculated and experimental values of the yield stress.

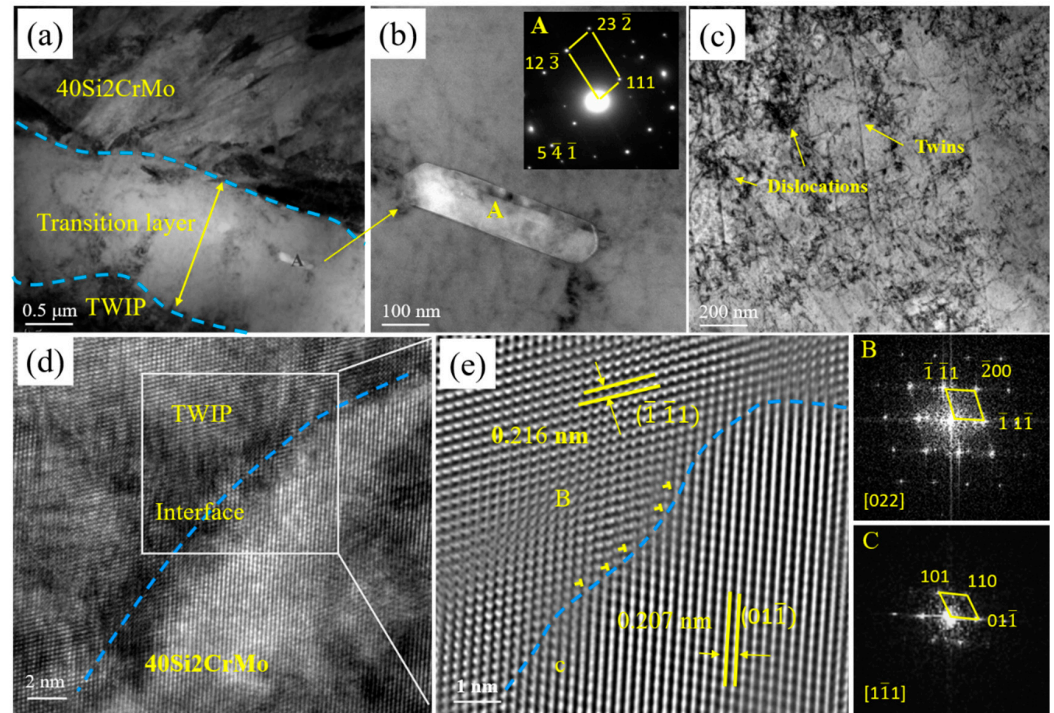
Sample	$\sigma_0$ (Mpa)	$\Delta\sigma_{\text{refin}}$ (Mpa)	$\Delta\sigma_{\text{twin}}$ (Mpa)	Calculated Value (MPa)	Experimental Value (MPa)
80%	728.5	95.3	53.6	877.4	865
90%	728.5	99.0	55.8	883.3	1028
95%	728.5	102.2	57.4	888.1	1148

Figure 13 shows the TEM analysis of the multilayer steel with a reduction hot rolling of 95%. As shown in Figure 13a, the boundary of the component layer/transition layer can be seen clearly, the thickness of the transition layer was about 2 microns, and some long strips of  $\text{Al}_2\text{O}_3$  oxides were formed (Figure 13b). Due to the difference in the lattice parameters between the two component layers, the interface contains many mismatched dislocations, as shown in Figure 13d,e, which will increase the distortion energy on the interface and can more effectively block the movement of dislocations and improve the strain hardening ability of the material. We found two sets of crystal plane orientations as follows:  $72^\circ$  angle, between TWIP ( $\bar{1}\bar{1}1$ ) and 40Si2CrMo (01 $\bar{1}$ ). The interplanar spacing of ( $\bar{1}\bar{1}1$ ) and (01 $\bar{1}$ ) were 0.577 nm and 0.707 nm, respectively. The mismatch degree of the

two-phase matching crystal planes at the phase boundary can be calculated according to the following formula [30]:

$$\delta = \frac{|d_{(01\bar{1})} - d_{(\bar{1}\bar{1}1)}|}{d_{(\bar{1}\bar{1}1)}} = 0.225 < 0.25 \quad (10)$$

where  $d_{(01\bar{1})}$  and  $d_{(\bar{1}\bar{1}1)}$  are interplanar spacings of  $(01\bar{1})$  and  $(\bar{1}\bar{1}1)$ , respectively.



**Figure 13.** TEM images of multilayer TWIP/40Si2CrMo steel with a hot rolling reduction of 95%: (a) interface area; (b) Oxides at the interface, A is selected area electron diffraction (SAED) of Figure (b); (c) TWIP steel layer; (d) interface HRTEM image; and (e) associated IFFT image of interface. B and C are FFT spots of the selected area of Figure (e).

That is to say part of the hetero interface atoms were in a semi-coherent relationship, compared with the incoherent interface, it was relatively stable and effective in storing dislocations due to the lower interface energy, which ensures the higher plasticity of the multilayer composite steels.

Combined with the previous results and discussion, it can be seen that the strengthening and toughening mechanism of multilayer TWIP/40Si2CrMo steel was the result of fine grain strengthening, work hardening, and load transfer caused by interface. With the increase of the hot rolling reduction, the grain size of TWIP/40Si2CrMo multilayer steel decreases slightly, while the dislocation density and deformation twins increase slightly, but these were not the main reasons for the synergistic enhancement of strength and plasticity. With the increase of hot rolling reduction, the gradually enhanced interfacial bond strength was the key factor that improved the mechanical properties, especially the plasticity of the multilayer steel. Figure 14 is a schematic diagram of the damage failure of multilayer steels with different hot rolling reductions. When the multilayer steel with a hot rolling reduction was 80%, the interface has many  $\text{Al}_2\text{O}_3$  oxides with larger dimensions. The  $\text{Al}_2\text{O}_3$  oxide at the interface forms holes and the continuous tensile stress causes the cracks nucleation at the holes and propagates along with the interface, resulting in interface delamination and lower interface bonding strength. The weak interface cannot effectively transmit the load [31], which in turn causes the premature failure of the multilayer steel. When the hot rolling reduction was increased to 90%, the interfacial bonding strength of the multilayer

steel increased due to the decrease of  $\text{Al}_2\text{O}_3$  oxides. Therefore, under the action of the interface, the advancing cracks of the multilayer steel were continuously deflected during deformation. The multiple crack propagation paths contribute to energy dissipation, which increases the plasticity of the multilayer steel [32]. When the hot rolling reduction was increased to 95%, the stronger bonding interface effectively delays the local necking of the hard 40Si2CrMo steel layer, and the  $\text{Al}_2\text{O}_3$  oxide at the interface was further reduced, reducing the energy of crack nucleation. In addition, the strong bonding interface can effectively inhibit crack propagation along the interface. The TWIP steel layer with better plasticity makes the crack passivated while the 40Si2CrMo steel layer forms multiple tunnel cracks, and a certain plastic zone was formed at the crack tip, which releases the crack tip stress and improves the plasticity of multilayer steels [33]. The size of the plastic zone can be obtained from the following Equation [34,35]:

$$r_p = \frac{1}{2} \times \left( \frac{K_{BC}}{\sigma_{ys}} \right)^2 \quad (11)$$

where  $r_p$  is the size of the plastic zone;  $K_{BC}$  is the fracture toughness of the hard phase layer; and  $\sigma_{ys}$  is the yield strength.

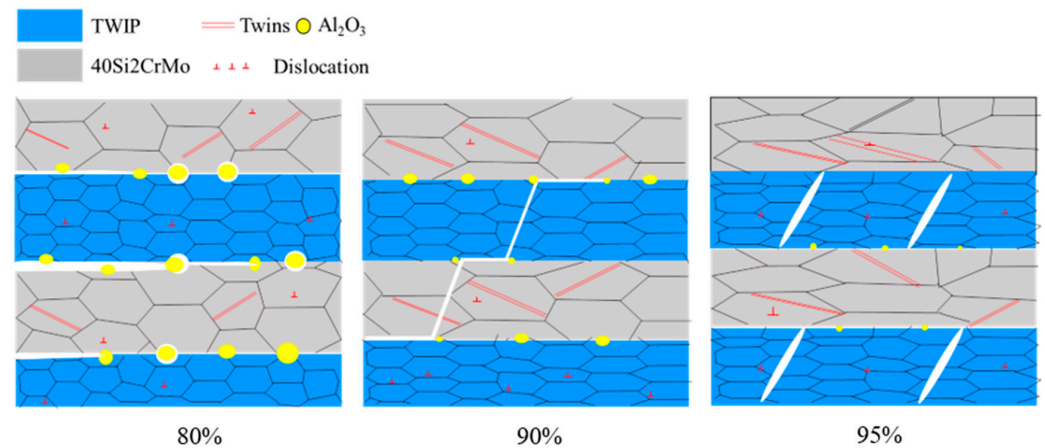


**Figure 14.** The schematic diagram of damage failure of multilayer steels with different hot rolling reductions.

In addition, with the increase of the hot rolling reduction, the layer thickness of multilayer steel decreases but the interface bonding strength increases. It has been reported that when the layer thickness was lower than the critical dimension of the tunnel crack, multiple tunnel cracks will be induced [14], so the fracture mode of the multilayer steels will change. The delamination fracture of the multilayer steel at low hot rolling reduction was transformed to the fracture mode that was dominated by tunnel cracks at a high hot rolling reduction, thereby improving the plasticity of the multilayer steel.

## 5. Conclusions

In this paper, three kinds of TWIP/40Si2CrMo multilayer steels with different layer thicknesses were successfully prepared by the vacuum hot rolling process. The main conclusions were as follows:

1. With the increase of the hot rolling reduction, the strength and plasticity of the multilayer steel were improved at the same time, breaking the trade-off relationship between the strength and plasticity of traditional metal materials. When the reduction was 95%, the yield strength, tensile strength, and fracture elongation of the multilayer steel increased to 1148 Mpa, 1311 MPa, and 27.8%, respectively, reaching the best strength and plasticity match. The increase in the strength was the result of grain refinement strengthening, work hardening, interface enhancement, and dislocation strengthening, while the increase in the

interfacial bonding strength and layer thickness scale effects lead to the optimization of toughness.

2. All the multilayer steels under different hot rolling reductions have relatively straight interfaces and good deformation coordination. With the increase of hot rolling reduction, the size and number of interfacial oxides decrease sharply, showing higher and higher interfacial bonding strength. This indicates that the hot rolling deformation was conducive to the breakage of oxides to make them appear dispersed and play a role in interfacial toughening.

3. The tensile fractures of multilayer steels with different hot rolling reductions show different fracture modes: delamination fracture and tunnel crack fracture. As the hot rolling reduction increases, the delamination fracture phenomenon weakens and the number of tunnel cracks increases, indicating that the interface bonding strength increases. At the same time, under the premise of a strong bonding interface and large reduction, the layer thickness decreases with increasing hot rolling reduction. When the layer thickness was lower than the critical dimension of tunnel cracks, this induced multiple tunnel cracks, which was conducive to the improvement of multilayer steel plasticity.

**Author Contributions:** Conceptualization, B.L.; methodology, W.Y.; software, Z.L.; validation, M.D.; formal analysis, C.C.; investigation, B.Y. and M.D.; resources, F.Y.; data curation, B.L.; writing-original draft preparation, M.D. and Z.L.; writing-review and edition, M.D.; project administration, C.C.; funding acquisition, F.Y. All authors have read and agreed to the published version of the manuscript.

**Funding:** The authors gratefully acknowledge the financial support from the Natural Science Foundation of Hebei, China (No. E2020202124, E2021202075), the foundation strengthening program (No: 2019-JCJQ-142-00), Key-Area R&D Program of Guangdong Province (2020B010134000), and Guangdong Academy of Science (2021GDASYL-20210102002).

**Data Availability Statement:** Not applicable.

**Conflicts of Interest:** We declare that we have no financial and personal relationships with other people or organizations that can inappropriately influence our work, and there are no professional or other personal interests of any nature or kind in any product, service, and/or company that could be construed as influencing the position presented in the review of the manuscript, entitled by "Interface strengthening and toughening mechanism of hot rolled multilayer TWIP/40Si2CrMo steels".

## References

1. Chen, L.; Zhao, Y.; Qin, X. Some Aspects of High Manganese Twinning-Induced Plasticity (TWIP) Steel, a Review. *Acta Metall. Sin. (Engl. Lett.)* **2013**, *26*, 1–15. [[CrossRef](#)]
2. Anand, K.K.; Mahato, B.; Haase, C.; Kumar, A.; Chowdhury, S.G. Correlation of Defect Density with Texture Evolution During Cold Rolling of a Twinning-Induced Plasticity (TWIP) Steel. *Mater. Sci. Eng. A* **2018**, *711*, 69–77. [[CrossRef](#)]
3. Hwang, J.-K. Effects of Caliber Rolling on Microstructure and Mechanical Properties in Twinning-Induced Plasticity (TWIP) Steel. *Mater. Sci. Eng. A* **2018**, *711*, 156–164. [[CrossRef](#)]
4. Wang, L.; Benito, J.A.; Calvo, J.; Cabrera, J.M. Equal Channel Angular Pressing of a TWIP Steel: Microstructure and Mechanical Response. *J. Mater. Sci.* **2017**, *52*, 6291–6309. [[CrossRef](#)]
5. Huang, M.; Chen, J.S.; Wu, H.; Fan, G.H.; Geng, L. Strengthening and Toughening of Layered Ti-Al Metal Composites by Controlling Local Strain Contribution. *IOP Conf. Ser. Mater. Sci. Eng.* **2017**, *219*, 012028. [[CrossRef](#)]
6. Ojima, M.; Inoue, J.; Nambu, S.; Xu, P.; Akita, K.; Suzuki, H.; Koseki, T. Stress Partitioning Behavior of Multilayered Steels During Tensile Deformation Measured by in Situ Neutron Diffraction. *Scr. Mater.* **2012**, *66*, 139–142. [[CrossRef](#)]
7. Pozuelo, M.; Carreño, F.; Ruano, O. Delamination Effect on the Impact Toughness of an Ultrahigh Carbon–Mild Steel Laminate Composite. *Compos. Sci. Technol.* **2006**, *66*, 2671–2676. [[CrossRef](#)]
8. Kang, J.; Kim, J.G.; Kim, S.; Chin, K.-G.; Lee, S.; Kim, H. Outstanding Mechanical Properties of High-Pressure Torsion Processed Multiscale TWIP-Cored Three Layer Steel Sheet. *Scr. Mater.* **2016**, *123*, 122–125. [[CrossRef](#)]
9. Koseki, T.; Inoue, J.; Nambu, S. Development of Multilayer Steels for Improved Combinations of High Strength and High Ductility. *Mater. Trans.* **2014**, *55*, 227–237. [[CrossRef](#)]
10. Seok, M.-Y.; Lee, J.-A.; Lee, D.-H.; Ramamurty, U.; Nambu, S.; Koseki, T.; Jang, J.-I. Decoupling the Contributions of Constituent Layers to the Strength and Ductility of a Multi-Layered Steel. *Acta Mater.* **2016**, *121*, 164–172. [[CrossRef](#)]
11. Zhang, B.; Liu, B.; He, J.; Ji, P.; Zhang, X.; Fang, W.; Feng, J.; Hu, X.; Yin, F. A New Route to Fabricate Multilayer Steel with Multiscale Hierarchical Structure. *Mater. Charact.* **2020**, *169*, 110606. [[CrossRef](#)]

12. Song, F.; Bai, Y.L. Effects of Nanostructures on the Fracture Strength of the Interfaces in Nacre. *J. Mater. Res.* **2003**, *18*, 1741–1744. [[CrossRef](#)]
13. Syn, C.K.; Lesuer, D.R.; Wolfenstine, J.; Sherby, O.D. Layer Thickness Effect on Ductile Tensile Fracture. *Metall. Mater. Trans. A* **1993**, *24*, 647–1653. [[CrossRef](#)]
14. Liu, B.; Huang, L.; Geng, L.; Wang, B.; Cui, X. Fracture Behaviors and Microstructural Failure Mechanisms of Laminated Ti–Tibw/Ti Composites. *Mater. Sci. Eng. A* **2014**, *611*, 290–297. [[CrossRef](#)]
15. Liu, B.; Huang, L.; Wang, B.; Geng, L. Effect of Pure Ti Thickness on the Tensile Behavior of Laminated Ti–Tibw/Ti Composites. *Mater. Sci. Eng. A* **2014**, *617*, 115–120. [[CrossRef](#)]
16. Liu, B.; Huang, L.; Geng, L.; Wang, B.; Liu, C.; Zhang, W. Fabrication and Superior Ductility of Laminated Ti–Tibw/Ti Composites by Diffusion Welding. *J. Alloy. Compd.* **2014**, *602*, 187–192. [[CrossRef](#)]
17. Wang, Y.; Chen, M.; Zhou, F.; Ma, E. High Tensile Ductility in a Nanostructured Metal. *Nature* **2002**, *419*, 912–915. [[CrossRef](#)]
18. Yang, M.; Yan, D.; Yuan, F.; Jiang, P.; Ma, E.; Wu, X. Dynamically Reinforced Heterogeneous Grain Structure Prolongs Ductility in a Medium-Entropy Alloy with Gigapascal Yield Strength. *Proc. Natl. Acad. Sci. USA* **2018**, *115*, 7224–7229. [[CrossRef](#)]
19. Ding, H.; Cui, X.; Wang, Z.; Zhao, T.; Wang, Y.; Zhang, Y.; Chen, H.; Huang, L.; Geng, L.; Chen, J. A New Strategy for Fabrication of Unique Heterostructured Titanium Laminates and Visually Tracking Their Synchronous Evolution of Strain Partitions Versus Microstructure. *J. Mater. Sci. Technol.* **2022**, *107*, 70–81. [[CrossRef](#)]
20. Yang, G.; Zhuang, C.; Li, C.; Lan, F.; Yao, H. Study on High-Temperature Mechanical Properties of Fe–Mn–C–Al TWIP/TRIP Steel. *Metals* **2021**, *11*, 821. [[CrossRef](#)]
21. Li, L.; Yin, F.; Tanaka, Y.; Kishimoto, S.; Nagai, K. Characteristics of the Cold-Rolling Texture in a Multi-Layered Material Composed of Sus301 and Sus420 Steels. *Mater. Trans.* **2010**, *51*, 911–917. [[CrossRef](#)]
22. Yu, W.; Liu, B.; He, J.; Chen, C.; Fang, W.; Yin, F. Microstructure Characteristics, Strengthening and Toughening Mechanism of Rolled and Aged Multilayer TWIP/Maraging Steels. *Mater. Sci. Eng. A* **2019**, *767*, 138426. [[CrossRef](#)]
23. Nambu, S.; Michiuchi, M.; Inoue, J.; Koseki, T. Effect of Interfacial Bonding Strength on Tensile Ductility of Multilayered Steel Composites. *Compos. Sci. Technol.* **2009**, *69*, 1936–1941. [[CrossRef](#)]
24. Inoue, J.; Nambu, S.; Ishimoto, Y.; Koseki, T. Fracture Elongation of Brittle/Ductile Multilayered Steel Composites with a Strong Interface. *Scr. Mater.* **2008**, *59*, 1055–1058. [[CrossRef](#)]
25. Williamson, G.K.; Hall, W.H. X-ray line broadening from filed aluminum and wolfram. *Acta Metall.* **1953**, *1*, 22–31. [[CrossRef](#)]
26. Sauzay, M.; Fournier, B.; Mottot, M.; Pineau, A.; Monnet, I. Cyclic Softening of Martensitic Steels at High Temperature-Experiments and Physically Based Modelling. *Mater. Sci. Eng. A* **2008**, *483–484*, 410–414. [[CrossRef](#)]
27. Chen, C.X.; Ge, Y.F.; Fang, W.; Zhang, X.; Liu, B.X.; Feng, J.H.; Yin, F.X. Multilayer Maraging/Cocnri Composites with Synergistic Strengthening-Toughening Behavior. *Front. Mater.* **2021**, *7*, 619315. [[CrossRef](#)]
28. Lee, S.-J.; Sun, Y.; Fujii, H. Stacking-Fault Energy, Mechanical Twinning and Strain Hardening of Fe-18mn-0.6c-(0, 1.5)Al Twinning-Induced Plasticity Steels During Friction Stir Welding. *Acta Mater.* **2018**, *148*, 235–248. [[CrossRef](#)]
29. Dolzhenko, A.; Pydrin, A.; Gaidar, S.; Kaibyshev, R.; Belyakov, A. Microstructure and Strengthening Mechanisms in an Hsla Steel Subjected to Tempforming. *Metals* **2021**, *12*, 48. [[CrossRef](#)]
30. Qian, S.Y.; Xu, Z.H.; Xie, H.N.; Shi, C.S.; Zhao, N.Q.; He, C.N.; Liu, E.Z. Effect of Rare Metal Element Interfacial Modulation in Graphene/Cu Composite with High Strength, High Ductility and Good Electrical Conductivity. *Appl. Surf. Sci.* **2020**, *533*, 147489. [[CrossRef](#)]
31. Ding, Y.; Cao, R.; Yan, Y. Effects of Heat Treatment on Fracture Mechanism of Martensite/Austenite MIs Composite Plates by Hot Roll Bonding. *Mater. Sci. Eng. A* **2020**, *773*, 138727. [[CrossRef](#)]
32. Wadsworth, J. Ancient and Modern Steels and Laminated Composites Containing Steels. *Mater. Res. Soc.* **2002**, *27*, 980–987. [[CrossRef](#)]
33. Shi, P.; Li, R.; Li, Y.; Wen, Y.; Zhong, Y.; Ren, W.; Shen, Z.; Zheng, T.; Peng, J.; Liang, X.; et al. Hierarchical Crack Buffering Triples Ductility in Eutectic Herringbone High-Entropy Alloys. *Science* **2021**, *373*, 912–918. [[CrossRef](#)] [[PubMed](#)]
34. Cao, H.C.; Evans, A.G. On Crack Extension in Ductile/Brittle Laminates. *Acta Metall. Mater.* **1991**, *39*, 2997–3005. [[CrossRef](#)]
35. Liu, B.; Huang, L.; Geng, L.; Wang, B.; Cui, X. Effects of Reinforcement Volume Fraction on Tensile Behaviors of Laminated Ti–Tibw/Ti Composites. *Mater. Sci. Eng. A* **2014**, *610*, 344–349. [[CrossRef](#)]